Decaying sterile neutrinos and the short baseline oscillation anomalies

Mona Dentler,[1,*] Ivan Esteban,[2,†] Joachim Kopp,[3,4,‡] and Pedro Machado[5,§]

[1]*Institut für Astrophysik, Georg August-Universität Göttingen, 37077 Göttingen, Germany*
[2]*Departament de Fisíca Quàntica i Astrofísica and Institut de Ciencies del Cosmos, Universitat de Barcelona, 08028 Barcelona, Spain*
[3]*Theoretical Physics Department, European Organization for Nuclear Research, 1211 Geneva, Switzerland*
[4]*PRISMA Cluster of Excellence and Mainz Institute for Theoretical Physics, Johannes Gutenberg-Universität Mainz, 55128 Mainz, Germany*
[5]*Fermi National Accelerator Laboratory, Batavia, 60510 Illinois, USA*

(Received 18 November 2019; accepted 6 May 2020; published 11 June 2020)

The MiniBooNE experiment has observed a significant excess of electron neutrinos in a muon neutrino beam, in conflict with standard neutrino oscillations. We discuss the possibility that this excess is explained by a sterile neutrino with a mass ∼1 keV that decays quickly back into active neutrinos plus a new light boson. This scenario satisfies terrestrial and cosmological constraints because it has neutrino self-interactions built-in. Accommodating also the LSND, reactor, and gallium anomalies is possible, but requires an extension of the model to avoid cosmological limits.

DOI: 10.1103/PhysRevD.101.115013

I. INTRODUCTION

Many major discoveries in neutrino physics have started out as oddball anomalies that gradually evolved into incontrovertible evidence. In this work, we entertain the possibility that history is repeating itself in the context of the MiniBooNE anomaly. From 2002 to 2019, the MiniBooNE experiment has been searching for electron neutrinos (ν_e) appearing in a muon neutrino (ν_μ) beam [1–3],[1] and has found a corresponding signal at 4.8σ statistical significance. For some time, the simplest explanation for this signal appeared to be the existence of a fourth neutrino species ν_s, called "sterile neutrino" because it would not couple to any of the Standard Model interactions, but would communicate with the Standard Model only via neutrino mixing. If ν_s has small but nonzero mixing with both ν_e and ν_μ and if the corresponding mostly sterile neutrino mass eigenstate ν_4 is somewhat heavier (∼1 eV) than the Standard Model neutrinos, the MiniBooNE signal could be explained. This explanation would also be consistent with a similar 3.8σ anomaly from the earlier LSND experiment [4], and with several reported hints for anomalous disappearance of electron neutrinos in reactor experiments [5,6] and in experiments using intense radioactive sources [7,8].[2] However, the sterile neutrino parameter space consistent with MiniBooNE and these other anomalies is in severe tension with the nonobservation of anomalous ν_μ disappearance [9–19], unless several additional new physics effects are invoked concomitantly [20,21].

In this work, we propose a different explanation for the MiniBooNE anomaly, and possibly also for the LSND, reactor, and gallium anomalies. In particular, we consider a sterile neutrino that rapidly decays back into Standard Model ("active") neutrinos ν_a [22–24]. The MiniBooNE excess is then interpreted as coming from these decay products. We will see that this scenario requires only very small mixing between ν_s and ν_μ, thus avoiding the strong ν_μ disappearance constraints. It also requires somewhat larger mixing between ν_s and ν_e, in line with the hints from reactor and radioactive source experiments. Finally, we will argue that decaying sterile neutrinos may avoid cosmological constraints because the model automatically endows sterile neutrinos with self-interactions ("secret interactions" [25,26]).

II. DECAYING STERILE NEUTRINO FORMALISM

We extend the Standard Model by a sterile neutrino ν_s (a Dirac fermion) and a singlet scalar ϕ. The relevant

*monainge.dentler@uni-goettingen.de
†ivan.esteban@fqa.ub.edu
‡jkopp@cern.ch
§pmachado@fnal.gov

[1]Here and in the following, when we say neutrino we mean also the corresponding antineutrinos.

[2]The latter class of experiments is usually referred to as "gallium experiments," based on the active component of their target material.

interaction and mass terms in the Lagrangian of the model are

$$\mathcal{L} \supset -g\bar{\nu}_s\nu_s\phi - \sum_{a=e,\mu,\tau,s} m_{\alpha\beta}\bar{\nu}_\alpha\nu_\beta. \quad (1)$$

The neutrino flavor eigenstates ν_α are linear combinations of the mass eigenstates ν_j ($j = 1, 2, 3, 4$) according to the relation $\nu_\alpha = U_{\alpha j}\nu_j$, where U is the unitary 4×4 leptonic mixing matrix. The first term in Eq. (1) can thus be rewritten as

$$-g\bar{\nu}_F\nu_F\phi - g|U_{s4}|^2\bar{\nu}_4\nu_4\phi - (gU^*_{s4}\bar{\nu}_4\nu_F\phi + \text{H.c.}), \quad (2)$$

with

$$\nu_F \equiv \sum_{i=1}^{3} U_{si}\nu_i. \quad (3)$$

We assume initially that the fourth, mostly sterile, mass eigenstate $\nu_4 \simeq \nu_s$ has a mass m_4 between $\mathcal{O}$(eV) and $\mathcal{O}$(100 keV), and that the mass of ϕ is of the same order, but smaller. The last term in Eq. (2) will then induce $\nu_4 \to \nu_F + \phi$ decays, while the first term is responsible for $\phi \to \nu_F + \bar{\nu}_F$ decays. When these decays occur in a neutrino beam, they will produce lower-energy neutrinos at the expense of higher-energy ones, and they may also alter the flavor structure of the beam. In particular, they can produce excess low-energy ν_e in a ν_μ beam, as suggested by the MiniBooNE anomaly.

The phenomenology of the model depends mainly on five new parameters. Besides m_4 and m_ϕ, these are the coupling g and the mixings $|U_{e4}|^2$, $|U_{\mu 4}|^2$ between ν_4 and ν_e, ν_μ. We will assume the mixing with ν_τ to be zero and neglect the complex phases, as these parameters do not play an important role in explaining the MiniBooNE excess. For practical purposes, it is convenient to quote $m_4\Gamma_4$ instead of g, as $m_4\Gamma_4$ appears directly in the laboratory frame decay length $E/(m_4\Gamma_4)$. Also, it is convenient to use the ratio m_ϕ/m_4 instead of just m_ϕ because the ratio measures more directly the kinematic suppression in ν_4 decays.

The evolution in energy E and time t of a neutrino beam in our model can be described by a neutrino density matrix $\hat{\rho}_\nu(E,x)$ (a 4×4 matrix in flavor space), the corresponding antineutrino density matrix $\bar{\hat{\rho}}_\nu(E,x)$, and the scalar density function $\rho_\phi(E,t)$. The evolution equations are [27,28],

$$\frac{d\hat{\rho}_\nu(E,t)}{dt} = -i[\hat{H},\hat{\rho}_\nu] - \frac{1}{2}\left\{\frac{m_4}{E}\hat{\Gamma},\rho\right\} + \mathcal{R}_\nu[\hat{\rho}_\nu,\rho_\phi,E,t] \quad (4)$$

$$\frac{d\rho_\phi(E,t)}{dt} = -\frac{m_\phi}{E}\Gamma_\phi\rho_\phi + \mathcal{R}_\phi[\hat{\rho}_\nu,E,t] \quad (5)$$

where $\hat{H} = \frac{1}{2E}\text{diag}(0,\Delta m^2_{21},\Delta m^2_{31},\Delta m^2_{41})$ is the standard neutrino oscillation Hamiltonian, written here in the mass basis, and $\hat{\Gamma} = \Gamma_4\hat{\Pi}_4$ is the decay term, which contains the projection operator $\hat{\Pi}_4 = |\nu_4\rangle\langle\nu_4|$ onto the fourth, mostly sterile, mass eigenstate as well as the decay width Γ_4 of ν_4 in its rest frame. Similarly, Γ_ϕ is the rest frame decay width of ϕ. The functional $\mathcal{R}_\nu[\hat{\rho}_\nu,\rho_\phi,E,t]$ describes the appearance of the daughter neutrinos from ν_4 and ϕ decay. Neglecting the masses of ν_1, ν_2, and ν_3, it is given by

$$\begin{aligned}\mathcal{R}_\nu[\hat{\rho}_\nu,\rho_\phi,E,t] &= \hat{\Pi}_F\int_{\frac{E}{1-x^2_{\phi 4}}}^{\infty} dE_4 \sum_k \hat{\rho}_{\nu,44}(E_4,t)\frac{d\Gamma^{\text{lab}}(\nu_4\to\nu_k\phi)}{dE_k} \\ &\quad + \hat{\Pi}_F\sum_{k,j}\int_E^\infty dE_\phi\rho_\phi(E_\phi,t)\frac{d\Gamma^{\text{lab}}(\phi\to\nu_k\bar{\nu}_j)}{dE_k}, \end{aligned} \quad (6)$$

where $d\Gamma^{\text{lab}}(X\to Y)/dE_k$ are the differential decay widths for the various decays $X\to Y$ in the lab frame, and $x_{\phi 4} \equiv m_\phi/m_4$. The projection operator

$$\hat{\Pi}_F = \frac{|\nu_F\rangle\langle\nu_F|}{|\langle\nu_F|\nu_F\rangle|^2} = \sum_{i,j=1}^{3}\frac{U^*_{si}U_{sj}}{\sum_k|U_{sk}|^2}|\nu_i\rangle\langle\nu_j| \quad (7)$$

isolates the specific combination of mass eigenstates that appears in ν_4 and ϕ decays, and the integrals run over all parent energies E_4, E_ϕ that lead to daughter neutrinos of energy E. Analogously, $\mathcal{R}_\phi[\hat{\rho}_\nu,E,t]$ describes the appearance of scalars from ν_4 decay:

$$\begin{aligned}\mathcal{R}_\phi[\hat{\rho}_\nu,E,t] = \int_E^{E/x^2_{\phi 4}} dE_4\sum_k\Bigg[&\hat{\rho}_{\nu,44}(E_4,t)\frac{d\Gamma^{\text{lab}}(\nu_4\to\nu_k\phi)}{dE_\phi} \\ &+ \bar{\hat{\rho}}_{\nu,44}(E_4,t)\frac{d\Gamma^{\text{lab}}(\bar{\nu}_4\to\bar{\nu}_k\phi)}{dE_\phi}\Bigg]. \end{aligned} \quad (8)$$

With the appearance terms $\mathcal{R}_\nu[\hat{\rho}_\nu,\rho_\phi,E,t]$ and $\mathcal{R}_\phi[\hat{\rho}_\nu,E,t]$ defined, the equations of motion (4) and (5) can be solved analytically if we neglect matter effects. Neglecting furthermore the small mass splittings between the three light neutrino mass eigenstates, the electron neutrino flux $\phi_e(L,E)$ appearing in a muon neutrino beam of energy E after a distance L due to oscillations and decay is given by

$$\begin{aligned}\phi_e(L,E) = \phi_\mu(0,E)|U_{e4}|^2|U_{\mu 4}|^2\Bigg[&1 + e^{-\frac{m_4\Gamma_4 L}{E}} \\ &- 2e^{-\frac{m_4\Gamma_4 L}{2E}}\cos\left(\frac{\Delta m^2_{41}L}{2E}\right)\Bigg] + |U_{\mu 4}|^2\frac{|\langle\nu_e|\nu_F\rangle|^2}{|\langle\nu_F|\nu_F\rangle|^2}\mathcal{I}. \end{aligned} \quad (9)$$

Here, $|\nu_F\rangle$ is the superposition of mass eigenstates into which the ν_4 decay [defined in Eq. (3)], and the decay integral $\mathcal{I}$ is given by

$$\mathcal{I} = \int_{E/(1-x_{\phi 4}^2)}^{\infty} dE_4 (1 - e^{-\frac{m_4\Gamma_4 L}{E_4}}) \phi_\mu(0, E_4) \sum_j \frac{1}{\frac{m_4}{E_4}\Gamma_4} \frac{d\Gamma^{\rm lab}(\nu_4 \to \nu_j \phi)}{dE}$$
$$+ \int_E^{\infty} dE_\phi \int_{E_\phi}^{E_\phi/x_{\phi 4}^2} dE_4 \frac{1}{\frac{m_4\Gamma_4 L}{E_4} - \frac{m_\phi \Gamma_\phi L}{E_\phi}} \left[(1 - e^{-\frac{m_\phi \Gamma_\phi L}{E_\phi}}) \frac{m_4\Gamma_4 L}{E_4} - (1 - e^{-\frac{m_4\Gamma_4 L}{E_4}}) \frac{m_\phi \Gamma_\phi L}{E_\phi} \right]$$
$$\times \frac{1}{\frac{m_4}{E_4}\Gamma_4} \sum_j \left[\phi_\mu(0, E_4) \frac{d\Gamma^{\rm lab}(\nu_4 \to \nu_j \phi)}{dE} + \bar{\phi}_\mu(0, E_4) \frac{d\Gamma^{\rm lab}(\bar{\nu}_4 \to \bar{\nu}_j \phi)}{dE} \right] \sum_{i,j} \frac{1}{\frac{m_\phi}{E_\phi}\Gamma_\phi} \frac{d\Gamma^{\rm lab}(\phi \to \nu_i \bar{\nu}_j)}{dE}. \quad (10)$$

In the above equations, $\phi_\mu(0, E)$ and $\bar{\phi}_\mu(0, E)$ are the initial ν_μ and $\bar{\nu}_\mu$ fluxes, respectively. A completely analogous equation describes $\bar{\nu}_e$ appearance.

The physical interpretation of Eq. (9) is straightforward: the first term on the right-hand side describes $\nu_\mu \to \nu_e$ oscillations, altered by the removal of neutrinos at energy E due to ν_4 decay. In fact, this contribution matches the result of Ref. [29], on invisible ν_4 decay. The second term gives the contribution from neutrinos generated in ν_4 and ϕ decays. The factor $|U_{\mu 4}|^2$ arises because ν_4 is the only mass eigenstate that decays. It describes the amount of ν_4 in the ν_μ beam. The factor $|\langle \nu_e | \nu_F \rangle|^2 / |\langle \nu_F | \nu_F \rangle|^2$ is the probability of the decay product to be detected as an electron neutrino, and the integral $\mathcal{I}$ controls the energy distribution of the decay products.

Analytic expressions for the decay widths appearing in Eqs. (4)–(12) are given in Appendix B.

III. FIT TO MINIBOONE DATA

To compare the predictions of the decaying sterile neutrino scenario to MiniBooNE data, we evolve the unoscillated beam following the formulas given above. We then follow the fitting procedure recommended by the MiniBooNE collaboration (see the data releases accompanying Refs. [1,3]), but go beyond it by accounting for the impact of ν_μ and ν_e disappearance on the signal and background normalization (see Appendix for details).

Illustrative results are shown in Fig. 1, where we have chosen parameter values that give an optimal fit to MiniBooNE data while being consistent with null results from other oscillation experiments, as well as nonoscillation constraints. At $m_4\Gamma_4 = 2.1\text{eV}^2$, most ν_4 will have decayed before reaching the detector. The value $m_\phi/m_4 = 0.82$ implies mild phase space suppression in ν_4 decays, which tends to shift the ν_e spectrum to lower energies, in excellent agreement with the data. Compared to models with massless ϕ [22,23], our scenario also has the advantage that it allows $\phi \to \nu_F \bar{\nu}_F$ decays, further boosting the ν_e flux at low energies. It is therefore favored compared to the $m_\phi = 0$ case at more than 99% confidence level. The fit in our model is better than in oscillation-only scenarios (blue dotted histogram in Fig. 1) [19], which by themselves

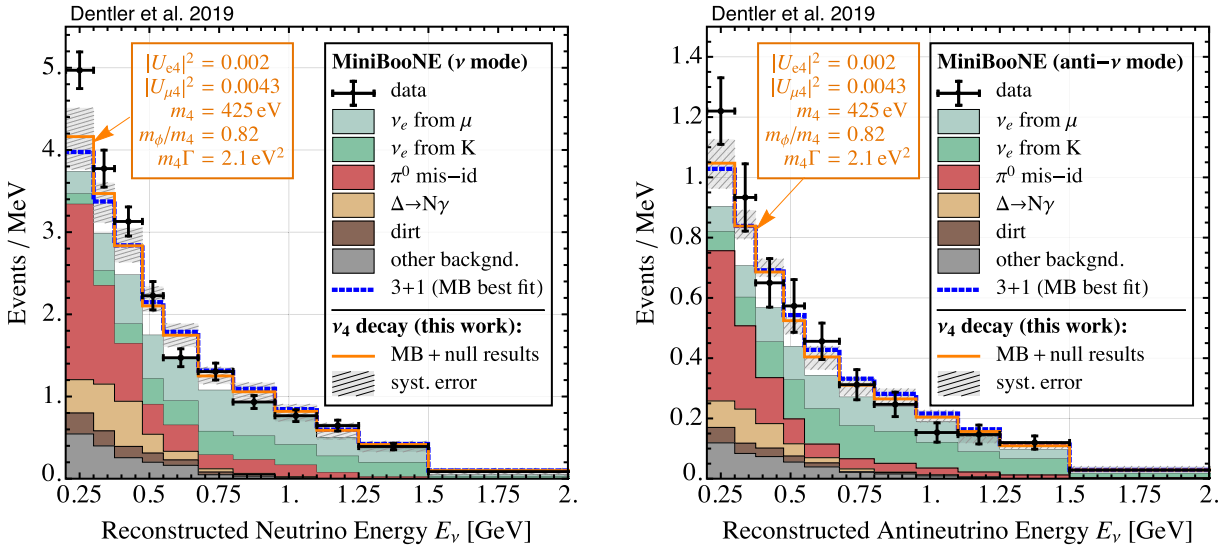

FIG. 1. Comparison of MiniBooNE neutrino-mode (left) and antineutrino-mode (right) data [3] to the predictions of the neutrino oscillation + decay scenario discussed in this work. We show the expected spectrum at the point which optimally fits MiniBooNE data, while being consistent with all null results (orange histogram with systematic error band; parameters given in the plot). We also show the MiniBooNE-only best point for $3+1$ oscillations without decay (blue dotted histogram, parameter values $\Delta m_{41}^2 = 0.13\ \text{eV}^2$, $|U_{e4}|^2 = 0.024$, $|U_{\mu 4}|^2 = 0.63$).

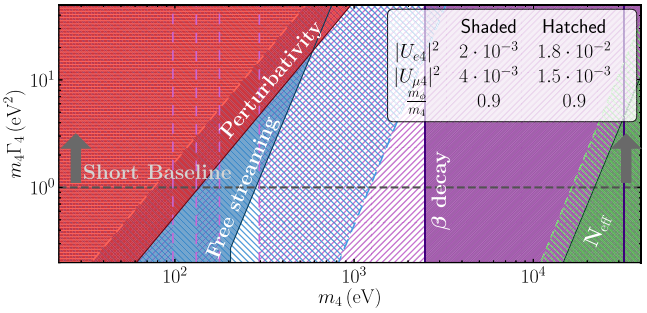

FIG. 2. Nonoscillation constraints on decaying sterile neutrinos for parameters favored by the global fit without LSND (shaded), and by the global fit without the free-streaming constraint (hatched).

already offer an excellent fit as long as only MiniBooNE data are considered (MiniBooNE quotes a χ^2 per degree of freedom of 9.9/6.7 [3]). Our model, however, is also consistent with all constraints. Notably, it reproduces the angular distribution of the neutrino interaction products in MiniBooNE because it predicts an actual flux of electron neutrinos instead of attempting to mimic the signal with other particles [30–35]. In particular, the angle between the parent ν_s and the daughter ν_e is suppressed by a large Lorentz boost $\gamma \sim \mathcal{O}(1000)$ [36]. This boost is sufficient to ensure that the daughter neutrinos enter the MiniBooNE detector, which is a ∼6 m sphere located ∼500 m from the primary target, under essentially the same angle as the parent neutrino would have done.

IV. CONSTRAINTS

We now discuss the various constraints that an explanation of the MiniBooNE anomaly in terms of decaying sterile neutrinos has to respect. The most relevant constraints are also summarized in Figs. 2 and 3.

(1) Oscillation null results. Putting MiniBooNE into context with other ν_e appearance searches, we show in Fig. 3 two slices through the 5-dimensional parameter space of the decaying sterile neutrino model along the plane spanned by $|U_{e4}|^2$ and $|U_{\mu4}|^2$. To produce this figure, we have used fitting codes from Refs. [9,12,19] (based partly on Refs. [37–39]). We see that most of the parameter region preferred by MiniBooNE is well compatible with the KARMEN short-baseline oscillation search [40] and with the OPERA long-baseline experiment [41]. We have checked that the limits from ICARUS [42–44] and E776 [45] are significantly weaker.

All constraints on $|U_{e4}|^2$ ($|U_{\mu4}|^2$) from ν_e (ν_μ) disappearance experiments are avoided [17,19,46]. This is mostly because in pure oscillation scenarios the number of excess events in MiniBooNE and LSND is proportional

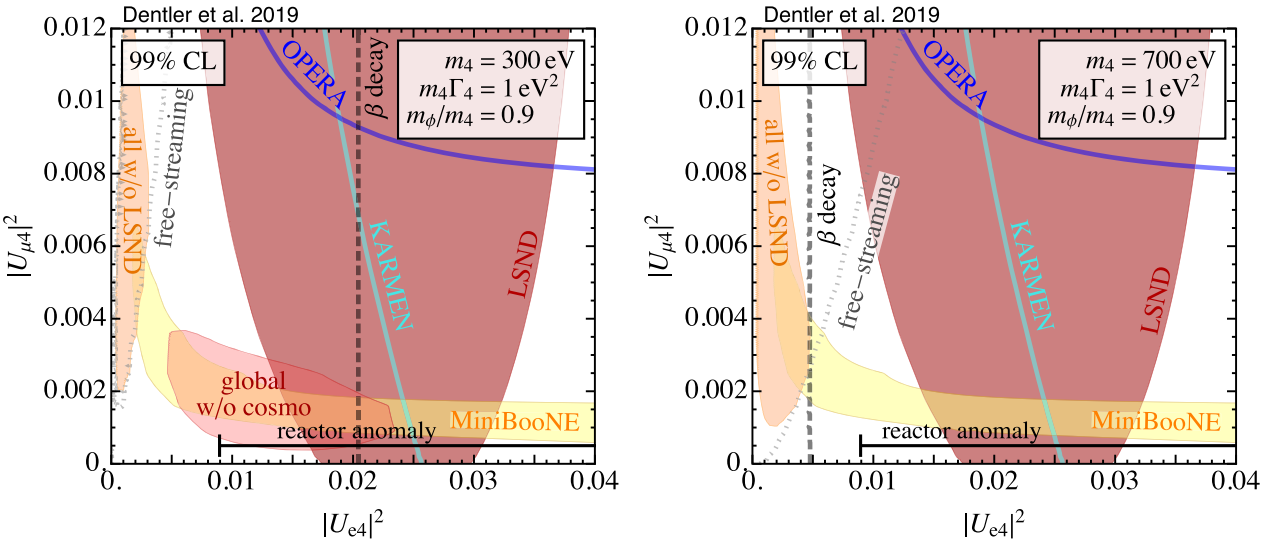

FIG. 3. Allowed values of the squared mixing matrix elements $|U_{e4}|^2$ and $|U_{\mu4}|^2$ (measuring the mixing of ν_s with ν_e and ν_μ, respectively) in the decaying sterile neutrino scenario. We show two representative slices through the 5-dimensional 99% confidence regions. Our fits include MiniBooNE, OPERA, ICARUS, E776, and KARMEN data, as well as constraints from nuclear beta decay spectra and from the requirement of neutrino free-streaming in the early Universe. For the null results from oscillation experiments, the region to the right of the curves is excluded. For the free-streaming constraint, the region to the left of the gray dotted contour is excluded. We also show, as a black rule at the bottom of the plot, the $|U_{e4}|^2$ range preferred by the reactor neutrino anomaly. Constraints on ν_μ disappearance are significantly weaker here than in the $3+1$ scenario without decay, and are hence not shown. We also do not show a fit including both LSND and cosmology as the goodness of fit would be very poor. Note that the global combinations are sensitive to five degrees of freedom, namely m_4, $|U_{e4}|^2$, $U^2_{\mu4}$, $m_4\Gamma_4$, and m_ϕ/m_4; oscillation experiments are sensitive only to the last four of these; beta decay spectra depend on two degrees of freedom (m_4 and $|U_{e4}|^2$); reactor experiments depend only on $|U_{e4}|^2$; and the free-streaming constraint depends only on the parameter combination $m_4/|U_{s1}|$.

to $|U_{e4}|^2|U_{\mu 4}|^2$, while in our scenario it is proportional only to $|U_{\mu 4}|^2$ as long as $|U_{e4}|^2 \gg |U_{\mu 4}|^2$. Therefore, it agrees well even with the tightest constraints [47,48].

We can already see from Fig. 3 that MiniBooNE is also compatible with LSND and with the $|U_{e4}|^2$ range preferred by the reactor anomaly, but only in a parameter region that would unacceptably reduce free-streaming of active neutrinos in the early Universe. We will see below that this tension can be avoided in extensions of the model.

(2) Beta decay spectra (purple regions in Fig. 2 and black dashed lines in Fig. 3). Direct searches for sterile neutrinos looking for anomalous features in beta decay spectra [49–52] suggest that $\mathcal{O}(0.001-0.01)$ mixings between active and sterile neutrinos—as required by MiniBooNE—are allowed for $m_4 \lesssim$ few keV.

(3) Neutrinoless double beta decay. If neutrinos are Majorana particles, the nonobservation so far of neutrinoless double beta decay requires $m_4|U_{e4}|^2 \lesssim 0.2$ eV [53]. This is the reason we always focus on Dirac neutrinos in this work.

(4) $N_{\rm eff}$, a measure for the *energy density of relativistic particles in the early Universe* (green region in Fig. 2). The measured value of $N_{\rm eff}$ is very close to the SM value of ~ 3 both at the BBN and recombination epochs [54,55]. Naively, one might expect that this observation precludes the existence of a fourth neutrino species with $m_4 \lesssim$ MeV. In our model, however, the $N_{\rm eff}$ constraint is avoided by the "secret interactions" mechanism [25,26]: any small abundance of ν_s generates a temperature-dependent potential $V_{\rm eff} \propto g^2 T$, reducing the ν_s–ν_a mixing by a factor $\sqrt{\Delta m^2/(E V_{\rm eff})}$. Hence, the production of ν_s is suppressed until the temperature drops low enough. For the parameter range that the short-baseline anomalies are pointing to, this can easily be postponed to late times ($T \ll$ MeV), after neutrino-electron decoupling. Consequently, when ν_s are eventually produced, they are produced at the expense of active neutrinos, so $N_{\rm eff}$ does not change any more and constraints are automatically satisfied. More quantitatively, $N_{\rm eff}$ constraints are avoided when

$$(m_4\Gamma_4)^{\rm eff} \gtrsim 2\times 10^{-14}\ {\rm eV}^2 \left(\frac{m_4}{\rm eV}\right)^4, \tag{11}$$

where we have defined

$$(m_4\Gamma_4)^{\rm eff} \equiv \frac{m_4\Gamma_4}{|U_{s4}|^2(|U_{e4}|^2+|U_{\mu 4}|^2)\left(1-\frac{m_\phi^2}{m_4^2}\right)^2}. \tag{12}$$

This constraint can be easily satisfied in the mass range allowed by beta decay limits.

(5) $\sum m_\nu$, *the sum of neutrino masses.* Massive neutrinos affect the CMB as well as structure formation, and this has for instance allowed the Planck collaboration to set a limit $\sum m_\nu \lesssim 0.12$ eV [55]. In our model, this constraint is easily satisfied because in the interesting parameter range with $m_4 \gg 1$ eV and $m_4\Gamma_4 \gtrsim 1{\rm eV}^2$, any ν_4 that are produced in the early Universe will have decayed via $\nu_4 \to \nu_{1,2,3} + (\phi \to \nu_{1,2,3}\bar{\nu}_{1,2,3})$ long before recombination and the onset of structure formation.

(6) Neutrino free-streaming (blue region in Fig. 2 and gray dotted lines in Fig. 3). Via the mixing with ν_s, also the light neutrino mass eigenstates $\nu_{1,2,3}$ feel ϕ-mediated interactions and are therefore not fully free-streaming. This may put the model in tension with CMB observations, which require that neutrinos should free-stream from about redshift 10^5 onwards [56–60].[3] This requirement bounds the squared coupling among the lightest neutrino mass eigenstate and the scalar ϕ, i.e., $(g|U_{s1}|^2)^2$. (Heavier mass eigenstates are not relevant as they decay quickly.) Here we are taking ν_1 to be the lightest mass eigenstate, as favored by current data. Quantitatively,

$$(m_4\Gamma_4)^{\rm eff} \lesssim 4\times 10^{-10}\ {\rm eV}^2 \left(\frac{m_4}{\rm eV}\right)^4 \left(\frac{0.1}{|U_{s1}|}\right)^4 x_{\phi 4}^2. \tag{13}$$

with $m_4 \lesssim 200$ eV required for $g^2 \gtrsim 10^{-6}$ [60]. Note that in Fig. 3, this constraint is present even for very small mixings. This is because, at fixed $m_4\Gamma_4$, small mixings need to be compensated by a large coupling g, strengthening the free streaming constraint. The value of $|U_{s1}|^2$ is fixed in terms of $|U_{e1}|^2$ and $|U_{\mu 1}|^2$ by unitarity, assuming the active neutrino mixing angles to be fixed at their values from Ref. [66].

However, the constraint could be substantially weakened in extensions of our model, see for instance Refs. [67–70]. A minimalist example is the production of extra species of light particles at the expense of the neutrino sector after neutrino decoupling. These would compensate for the lack of free-streaming in active neutrinos.

(7) SN 1987A. The fact that neutrinos from supernova 1987A could be observed at Earth without being absorbed through scattering on the cosmic neutrino background constrains neutrino self-interactions [71]. We have checked that, due to mixing suppression, these constraints are avoided in our scenario. Note that supernova cooling, which is sensitive to noninteracting sterile neutrinos, does not constrain our model as ν_4 and ϕ quickly decay to lighter neutrinos that remain trapped in the supernova core.

(8) Decays of SM neutrinos. We have checked that decays of the form $\nu_{2,3} \to \bar{\nu}_1 + 2\nu_1$, mediated by an off-shell ϕ, are always sufficiently rare to be consistent with solar neutrino constraints [29,72]. Note, however, that we predict the cosmic neutrino background today to consist exclusively of ν_1 or ν_3, for normal and inverted neutrino mass ordering, respectively.

[3]It is noteworthy, though, that some cosmological fits have actually found a *preference* for neutrino self-interactions [56,61–65] that could be accommodated in our model.

(9) Perturbativity (red region in Fig. 2). Requiring that the ν_s–ϕ coupling constant g in Eqs. (1) and (2) is $< \sqrt{4\pi}$ imposes the bound

$$(m_4\Gamma_4)^{\text{eff}} \lesssim 0.25\ \text{eV}^2 \left(\frac{m_4}{\text{eV}}\right)^2. \tag{14}$$

Similarly to the free-streaming bound, this constraint applies even for very small mixing when $m_4\Gamma_4$ is fixed. This bound restricts m_4 in our model to be $\gtrsim$100 eV for $m_4\Gamma_4$ values large enough to explain the MiniBooNE anomaly.

In summary, the sterile neutrino mass range to explain the MiniBooNE anomaly is between 100 eV and 2.5 keV.

V. THE LSND AND REACTOR ANOMALIES

As shown in Fig. 3, decaying sterile neutrinos can simultaneously fit the MiniBooNE and LSND anomalies, but only if cosmological neutrino free-streaming constraints can be avoided (see discussion under point *(6)* above for possible scenarios). Quantitatively, a parameter goodness-of-fit test [73] reveals that LSND is incompatible with the rest of the data at the 4.7σ level if free-streaming constraints hold. If the free-streaming problem is solved by other means, this reduces to 2.1σ, implying consistency. The best fit to all data including LSND, but excluding free-streaming is found at $m_4 =$ 97 eV, $|U_{e4}|^2 = 0.018$, $|U_{\mu4}|^2 = 0.0015$, $m_4\Gamma_4 = 0.87\text{eV}^2$, $m_\phi/m_4 = 0.89$.

Interestingly, at this value of $|U_{e4}|^2$, the model can also explain the flux deficit observed in reactor and gallium experiments [5–8,19,74]. We test our model against reactor data by comparing to Daya Bay's generic flux-weighted cross section [75]. To estimate the viable parameter space we perform a chi-square-test using the covariance matrix given in the same reference. In addition we introduce a 2.4% systematic flux normalization error corresponding to the theoretical uncertainty, in accordance with Fig. 28 of Ref. [75]. The $|U_{e4}|^2$ region preferred by reactor experiments is included in Fig. 3, and a comparison of the reactor neutrino spectrum to our model prediction is shown in Fig. 4.

VI. DETAILED INVESTIGATION OF THE PARAMETER SPACE

To supplement Fig. 3 and give the reader a broader overview of the preferred parameter regions of decaying sterile neutrinos, we show in Figs. 5 and 6 additional slices through the 5-dimensional parameter space.

The color coding in the figure is the same as in Fig. 3: the yellow, banana-shaped regions are preferred by MiniBooNE, the large dark red ones by LSND; the orange regions at low $|U_{e4}|^2$ correspond to a global fit to MiniBooNE, OPERA, ICARUS, E776, KARMEN, nuclear

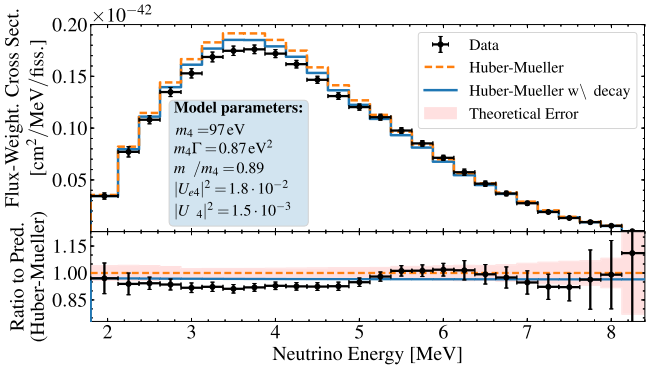

FIG. 4. Comparison of the reactor antineutrino spectrum predicted in the decaying sterile neutrino scenario discussed in this work (blue) to the standard Huber–Mueller prediction (orange-dashed) [76,77] and to Daya Bay data (black data points with error bars) [75]. For model parameters motivated by the MiniBooNE and LSND anomalies, a flux deficit consistent with the reactor anomaly can be accommodated. (See text for details, and for a discussion of how possible cosmological constraints can be avoided.)

beta decay spectra, and cosmological free-streaming constraints; bright red regions show instead a global fit to MiniBooNE, LSND, OPERA, ICARUS, E776, KARMEN, and nuclear beta spectra, but excluding the free-streaming constraint. Solid lines indicate constraints from OPERA (blue), ICARUS (purple), KARMEN (cyan), E776 (green), nuclear beta decay spectra (black dashed), and free-streaming in the early Universe (black dotted). The region to the right of the lines is excluded.

We observe that, at smaller values of $m_4\Gamma_4$, the allowed parameter regions from short-baseline oscillations (MiniBooNE, LSND, KARMEN) shift towards larger values of $|U_{e4}|^2$ and $|U_{\mu4}|^2$. In this case, only a small fraction of neutrinos decays before reaching the detector, making the phenomenology more similar to that of $3+1$ models without decay. Strong constraints from beta decay spectra and from cosmology imply that a good global fit cannot be achieved at $m_4\Gamma_4 \ll 1\ \text{eV}^2$.

Regarding the dependence of the fit on m_4, we note that smaller values of m_4 are favored by beta decay spectra, but disfavored by cosmology, in agreement with Fig. 2. Exclusion limits from oscillation experiments do not depend on m_4 for $m_4 \gg$ eV.

Comparing Fig. 5 with $m_\phi/m_4 = 0.5$ and Fig. 5 with $m_\phi/m_4 = 0.9$, we see that it becomes in general more difficult to fit all experiments at smaller m_ϕ/m_4. The reason is that, at small m_ϕ/m_4, the active neutrinos produced in ν_4 and ϕ decays have a harder spectrum. This in particular makes it more difficult to explain the MiniBooNE low-energy excess. In fact, for even smaller values of m_ϕ/m_4, and in particular for nearly massless ϕ (as considered in Refs. [22,23]), the MiniBooNE-preferred region would disappear completely from the plots.

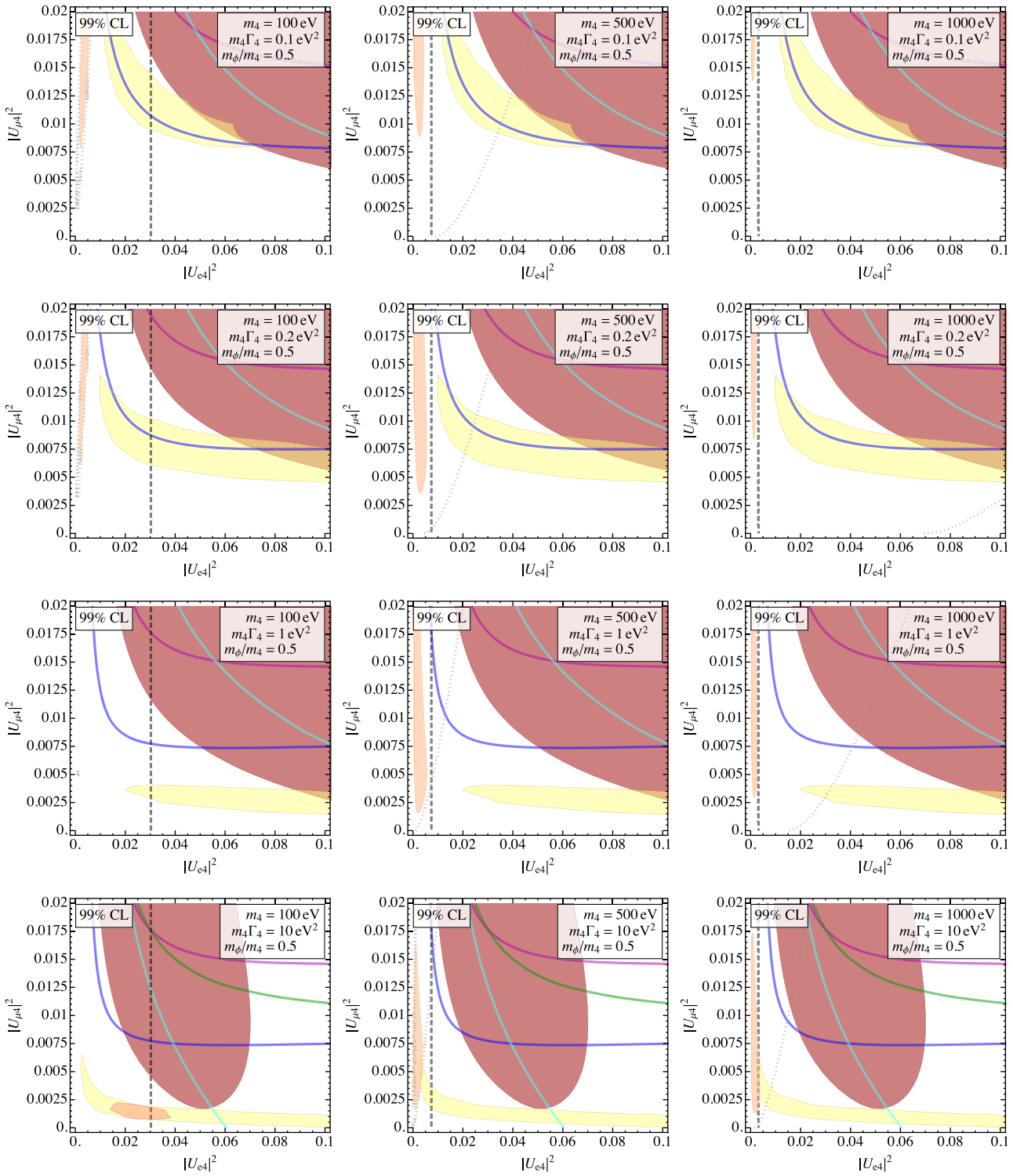

FIG. 5. Slices through the 5-dimensional parameter space of decaying sterile neutrinos at $m_\phi/m_4 = 0.5$ fixed. The color code is the same as in Fig. 3.

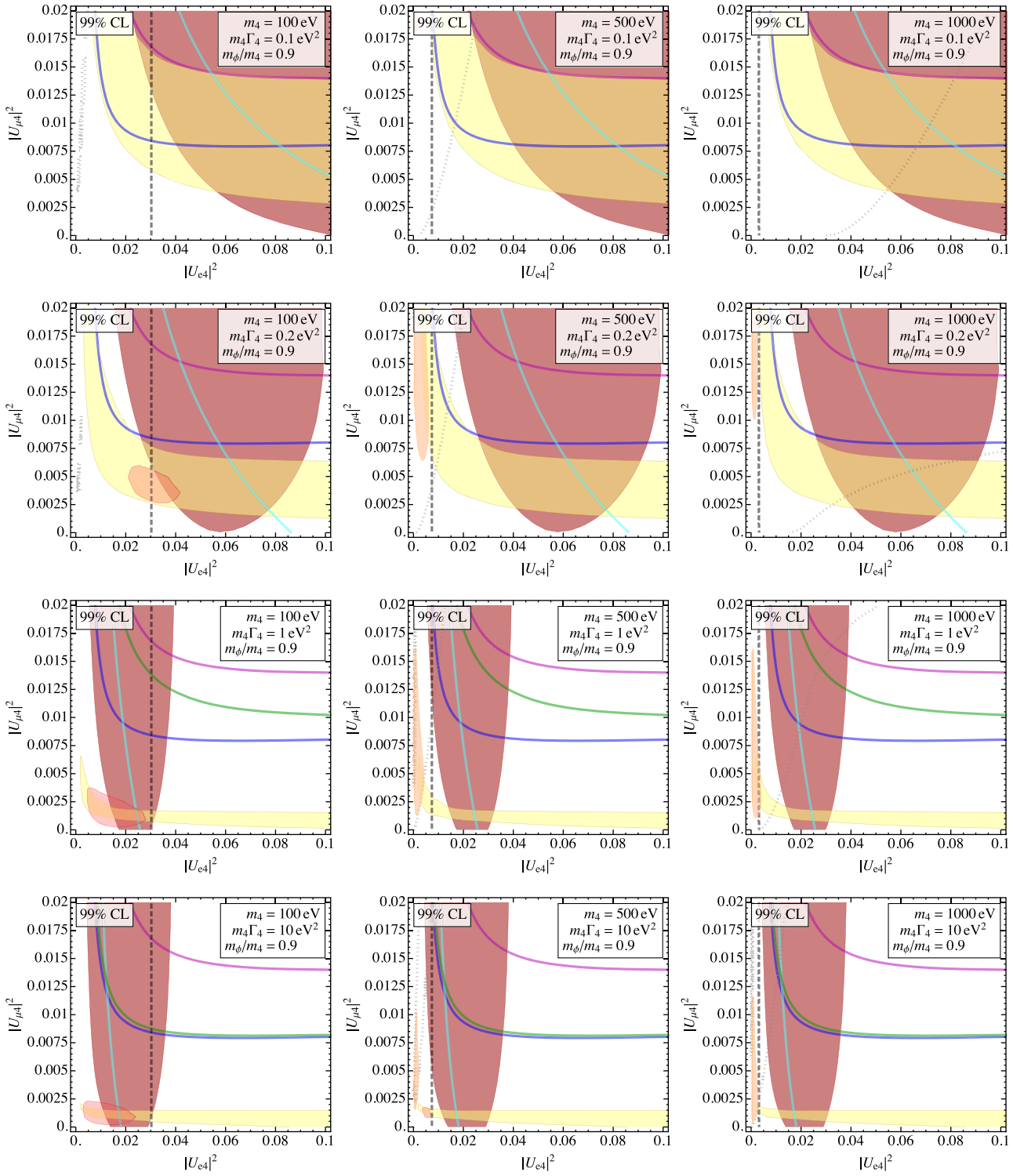

FIG. 6. Slices through the 5-dimensional parameter space of decaying sterile neutrinos at $m_\phi/m_4 = 0.9$ fixed. The color code is the same as in Fig. 3.

VII. CONCLUSIONS

In summary, we have shown that scenarios in which the SM is extended by a sterile neutrino that has a decay mode to active neutrinos can well explain the MiniBooNE anomaly without violating any constraints. An explanation of the LSND and reactor/gallium anomalies is possible if the model is extended to avoid constraints on neutrino free-streaming in the early Universe. The preferred mass of the sterile neutrino is of order few hundred eV.

ACKNOWLEDGMENTS

We would like to thank André de Gouvea, Frank Deppisch, Matheus Hostert, Bill Louis, and Michele Maltoni for very helpful discussions. We are particularly grateful to Thomas Schwetz for sharing his fitting codes, from which some of our own codes took inspiration. We also thank André de Gouvea, O. L. G. Peres, Suprabh Prakash and G. V. Stenico for sharing their draft on a similar neutrino decay solution to the SBL anomalies [24]. We thank Miguel Escudero and Samuel J. Witte for sharing their cosmological constraint. I. E. would like to thank CERN and Johannes Gutenberg University Mainz for their kind hospitality. This work has been funded by the German Research Foundation (DFG) under Grant Nos. EXC-1098, KO 4820/1–1, FOR 2239, GRK 1581, and by the European Research Council (ERC) under the European Union's Horizon 2020 research and innovation programme (grant agreement No. 637506, "νDirections"). Fermilab is operated by Fermi Research Alliance, LLC under contract No. DE-AC02-07CH11359 with the United States Department of Energy. I. E. acknowledges support from the FPU program fellowship FPU15/03697, the EU Networks FP10ITN ELUSIVES (H2020-MSCA-ITN-2015-674896) and INVISIBLES-PLUS (H2020-MSCA-RISE-2015-690575), and the MINECO Grant No. FPA2016-76005-C2-1-P. M. D. is supported by the Alexander von Humboldt Foundation and the German Federal Ministry of Education and Research.

APPENDIX A: IMPACT OF OSCILLATIONS ON THE BACKGROUND PREDICTION IN MINIBOONE

In this appendix, we briefly discuss our fit to MiniBooNE data, and in what ways it differs from the collaborations' fit as described in the supplemental material to Ref. [1], and using the data released with Ref. [3]. In particular, we consider the following three effects, which are relevant in a fit to a $3+1$ scenario, but are not encountered in a 2-flavor fit.

(1) Normalization of the $\nu_\mu \to \nu_e$ oscillation signal. To predict the number of expected ν_e events from $\nu_\mu \to \nu_e$ oscillations for a given set of oscillation parameters, the initial ν_μ flux must be known. It is obtained *in situ* using MiniBooNE's own sample of ν_μ events. Note, however, that in a $3+1$ model, the measured ν_μ flux will be reduced by an amount $\sim|U_{\mu 4}|^2$ due to $\nu_\mu \to \nu_s$ oscillations. (This effect is unimportant in a 2-flavor model, where the deficit is only of order $\sin^2 2\theta_{\mu e}$, where $\theta_{\mu e}$ is the effective 2-flavor mixing angle.) We account for this effect by first computing the expected ν_e signal based on the unoscillated MiniBooNE flux, and then diving it by the ν_μ survival probability in each bin.

The impact of this change in normalization is illustrated in the top panels of Fig. 7. The colored region in panel (a) of this figure shows our reproduction of the official MiniBooNE fit, which is shown as black contours. In panel (b), we have included the change in normalization for the signal.

(2) Oscillations of the ν_e backgrounds. Part of the MiniBooNE background is constituted by the intrinsic ν_e contamination in the beam. In a 2-flavor fit, this contribution to the total event rate is only modified by a factor of order $\sin^2 2\theta_{\mu e}$, but in the full $3+1$ framework, it is reduced by a factor of order $|U_{e4}|^2$ instead. The impact of this modification to the background sample is shown in Fig. 7(c).

(3) Oscillations of the ν_μ sample. The fit described in the supplemental material to Ref. [1] which we are following includes also MiniBooNE's sample of ν_μ events. This is necessary to properly account for systematic uncertainties which are correlated between the two samples. But of course, in a $3+1$ scenario, the ν_μ sample suffers from ν_μ disappearance into ν_s, proportional to $|U_{\mu 4}|^2$. (Once again, in a 2-flavor model, only a much smaller fraction $\propto \sin^2 2\theta_{\mu e}$ will disappear, which is usually negligible.) The impact of including ν_μ disappearance is shown in panel (d) of Fig. 7.

We see that including the effect of $3+1$ oscillations on the normalization in the control regions and on the background prediction reduces the significance of the MiniBooNE anomaly, though it remains above 3σ. These effects are thus unable to fully explain the MiniBooNE anomaly, but they could well be part of an "Altarelli cocktail" of several effects conspiring to lead to the large observed excess [78].

Let us finally mention one caveat with the above corrections to the MiniBooNE fit. Namely, we can only apply the corrections at the level of reconstructed events as the mapping between true and reconstructed neutrino energies is not publicly available for muon neutrinos. This means we have to assume that the reconstructed neutrino energy is a faithful representation of the true neutrino energy. While this is true for quasielastic scattering events which constitute the majority of events, it is not the case for other event categories. For instance, a neutrino–nucleon interaction may create an extra pion, and if this pion is reabsorbed as it propagates out of the nucleus, the

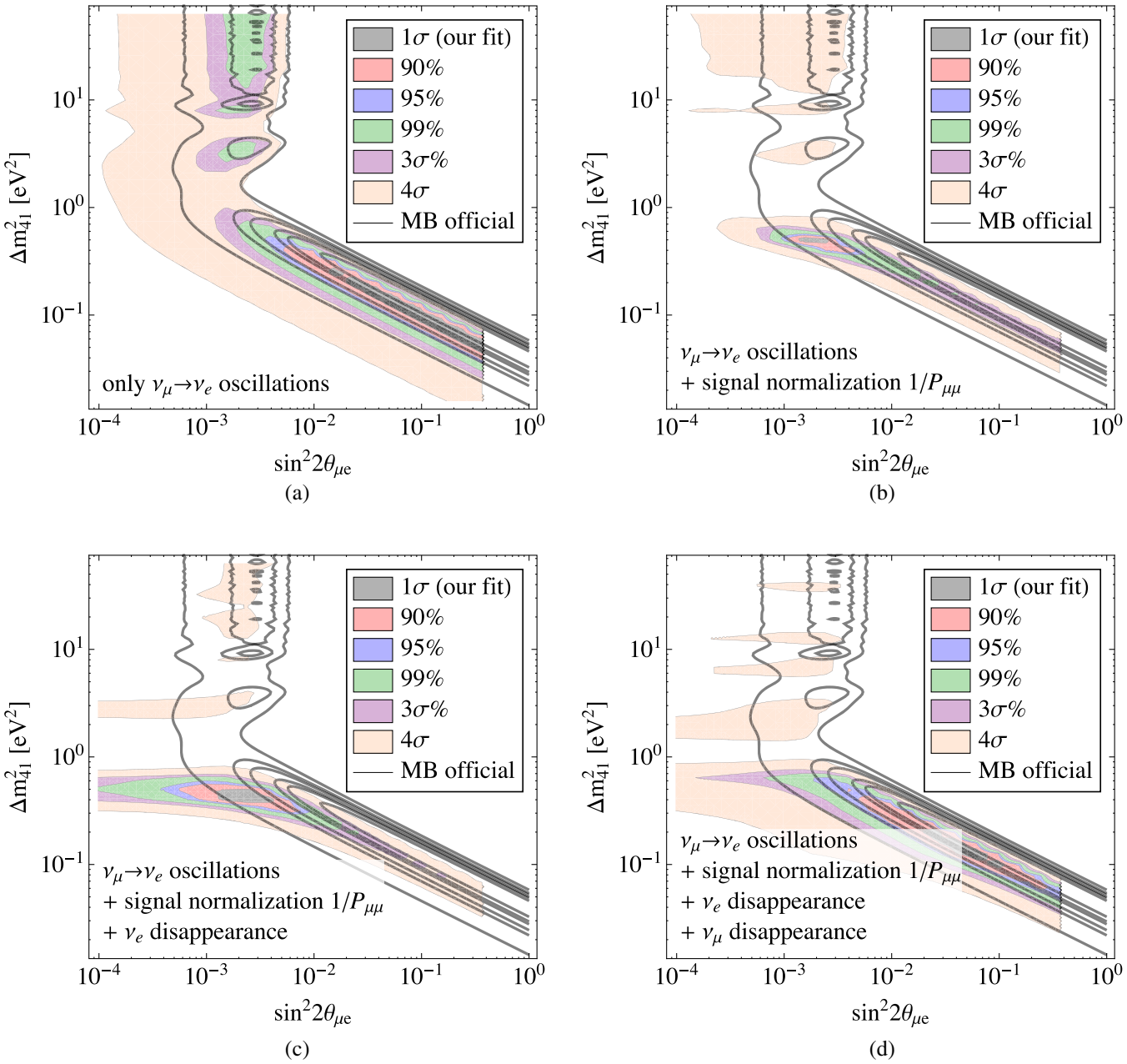

FIG. 7. Impact of oscillations in the background and control regions on the MiniBooNE fit in a simple 3 + 1 model (oscillations only, no decay). All panels show Δm^2_{41} vs the effective 2-flavor mixing angle $\sin^2 2\theta_{\mu e}$, which in a 3 + 1 scenario is given by $4|U_{e4}|^2|U_{\mu 4}|^2$. Panel (a) shows our reproduction (colored regions) of the official MiniBooNE fit (black contours), based on the instructions given in the supplemental material to Ref. [1] and using the data released with Ref. [3]. In panel (b), we include in addition the impact of $\nu_\mu \to \nu_s$ disappearance on the normalization of the signal in each bin. The colored contours in panel (c) include on top of this the effect of ν_s disappearance on the intrinsic ν_e contamination in the beam. Panel (d) finally shows the additional impact of ν_μ disappearance on the sample of ν_μ events that is included in the fit along with the ν_e sample. In all panels, we show projections of the three-dimensional parameter space spanned by Δm^2_{41}, $|U_{e4}|^2$, and $U_{\mu 4}|^2$ onto the Δm^2_{41}–$\sin^2 2\theta_{\mu e}$ plane, imposing the constraint $|U_{e4}|^2 < 0.2$ due to bounds from reactor neutrino experiments.

event will be misinterpreted as a quasi-elastic interaction, and the kinematic reconstruction of the neutrino energy based on the observed charged lepton energy and direction will fail.

APPENDIX B: DECAY WIDTHS AND TRANSITION PROBABILITY

Based on the interaction terms from Eq. (2), we can compute the differential decay rates of the heavy neutrino

ν_4 and of the scalar ϕ. In the massless light neutrino limit, we obtain for the ν_4 decay width in the lab

$$\frac{1}{\frac{m_4}{E_4}\Gamma_4}\frac{d\Gamma^{\rm lab}(\nu_4\to\nu_j\phi)}{dE_j}=\frac{|U_{sj}|^2}{\sum_{k=1}^3|U_{sk}|^2}\frac{E_j}{(1-x_{\phi 4}^2)^2E_4^2}, \tag{B1}$$

$$\sum_j\frac{1}{\frac{m_4}{E_4}\Gamma_4}\frac{d\Gamma^{\rm lab}(\nu_4\to\nu_j\phi)}{dE_\phi}=\frac{1}{1-x_{\phi 4}^2}\frac{1}{E_4}. \tag{B2}$$

In these expressions,

$$\Gamma_4=\frac{g^2}{16\pi}m_4(1-x_{\phi 4}^2)^2\sum_{j=1}^3|U_{s4}^*U_{sj}|^2 \tag{B3}$$

is the total rest frame decay width of ν_4, $x_{\phi 4}\equiv m_\phi/m_4$ is the ratio of scalar and neutrino masses, and E_j, E_ϕ are the daughter neutrino and scalar energies, respectively. In the ν_4 rest frame, E_j is restricted to the interval $[0, m_4(1-x_{\phi 4}^2)]$.

The lab frame decay rate of the scalar ϕ is

$$\sum_{i,j}\frac{1}{\frac{m_\phi}{E_\phi}\Gamma_\phi}\frac{d\Gamma^{\rm lab}(\phi\to\nu_i\bar\nu_j)}{dE_i}=\frac{1}{E_\phi}, \tag{B4}$$

with the total rest frame decay width of ϕ

$$\Gamma_\phi=\frac{g^2}{8\pi}m_\phi\sum_{i,j=1}^3|U_{si}^*U_{sj}|^2. \tag{B5}$$

The kinematic constraint on the daughter neutrino energies is $E_i, E_j\in[0, m_\phi]$.

[1] A. Aguilar-Arevalo *et al.* (MiniBooNE Collaboration), Event Excess in the MiniBooNE Search for $\bar\nu_\mu\to\bar\nu_e$ Oscillations, Phys. Rev. Lett. **105**, 181801 (2010).

[2] A. Aguilar-Arevalo *et al.* (MiniBooNE Collaboration), Improved Search for $\bar\nu_\mu\to\bar\nu_e$ Oscillations in the MiniBooNE Experiment, Phys. Rev. Lett. **110**, 161801 (2013).

[3] A. A. Aguilar-Arevalo *et al.* (MiniBooNE Collaboration), Observation of a Significant Excess of Electron-Like Events in the MiniBooNE Short-Baseline Neutrino Experiment, Phys. Rev. Lett. **121**, 221801 (2018).

[4] A. Aguilar *et al.* (LSND Collaboration), Evidence for neutrino oscillations from the observation of $\bar\nu_e$ appearance in a $\bar\nu_\mu$ beam, Phys. Rev. D **64**, 112007 (2001).

[5] G. Mention, M. Fechner, T. Lasserre, T. A. Mueller, D. Lhuillier, M. Cribier, and A. Letourneau, The reactor antineutrino anomaly, Phys. Rev. D **83**, 073006 (2011).

[6] M. Dentler, Á. Hernández-Cabezudo, J. Kopp, M. Maltoni, and T. Schwetz, Sterile neutrinos or flux uncertainties?—Status of the reactor anti-neutrino anomaly, J. High Energy Phys. 11 (2017) 099.

[7] M. A. Acero, C. Giunti, and M. Laveder, Limits on nu(e) and anti-nu(e) disappearance from Gallium and reactor experiments, Phys. Rev. D **78**, 073009 (2008).

[8] C. Giunti and M. Laveder, Statistical significance of the gallium anomaly, Phys. Rev. C **83**, 065504 (2011).

[9] J. Kopp, M. Maltoni, and T. Schwetz, Are There Sterile Neutrinos at the eV Scale?, Phys. Rev. Lett. **107**, 091801 (2011).

[10] J. Conrad, C. Ignarra, G. Karagiorgi, M. Shaevitz, and J. Spitz, Sterile neutrino fits to short baseline neutrino oscillation measurements, Adv.High Energy Phys. **2013**, 163897 (2013).

[11] M. Archidiacono, N. Fornengo, C. Giunti, S. Hannestad, and A. Melchiorri, Sterile neutrinos: Cosmology vs short-baseline experiments, Phys. Rev. D **87**, 125034 (2013).

[12] J. Kopp, P. A. N. Machado, M. Maltoni, and T. Schwetz, Sterile neutrino oscillations: The global picture, J. High Energy Phys. 05 (2013) 050.

[13] A. Mirizzi, G. Mangano, N. Saviano, E. Borriello, C. Giunti, G. Miele, and O. Pisanti, The strongest bounds on active-sterile neutrino mixing after Planck data, Phys. Lett. B **726**, 8 (2013).

[14] C. Giunti, M. Laveder, Y. Li, and H. Long, Pragmatic view of short-baseline neutrino oscillations, Phys. Rev. D **88**, 073008 (2013).

[15] S. Gariazzo, C. Giunti, and M. Laveder, Light sterile neutrinos in cosmology and short-baseline oscillation experiments, J. High Energy Phys. 11 (2013) 211.

[16] G. H. Collin, C. A. Argüelles, J. M. Conrad, and M. H. Shaevitz, Sterile neutrino fits to short baseline data, Nucl. Phys. **B908**, 354 (2016).

[17] S. Gariazzo, C. Giunti, M. Laveder, and Y. F. Li, Updated global 3 + 1 analysis of short-baseline neutrino oscillations, J. High Energy Phys. 06 (2017) 135.

[18] C. Giunti, X. P. Ji, M. Laveder, Y. F. Li, and B. R. Littlejohn, Reactor fuel fraction information on the antineutrino anomaly, J. High Energy Phys. 10 (2017) 143.

[19] M. Dentler, Á. Hernández-Cabezudo, J. Kopp, P. A. N. Machado, M. Maltoni, I. Martinez-Soler, and T. Schwetz, Updated global analysis of neutrino oscillations in the presence of eV-scale sterile neutrinos, J. High Energy Phys. 08 (2018) 010.

[20] J. Liao, D. Marfatia, and K. Whisnant, MiniBooNE, MINOS+ and IceCube data imply a baroque neutrino sector, Phys. Rev. D **99**, 015016 (2019).

[21] M. H. Moulai, C. A. Argüelles, G. H. Collin, J. M. Conrad, A. Diaz, and M. H. Shaevitz, Combining sterile neutrino fits to short baseline data with IceCube Data, Phys. Rev. D **101**, 055020 (2020).
[22] S. Palomares-Ruiz, S. Pascoli, and T. Schwetz, Explaining LSND by a decaying sterile neutrino, J. High Energy Phys. 09 (2005) 048.
[23] Y. Bai, R. Lu, S. Lu, J. Salvado, and B. A. Stefanek, Three twin neutrinos: Evidence from LSND and MiniBooNE, Phys. Rev. D **93**, 073004 (2016).
[24] A. de Gouvêa, O. L. G. Peres, S. Prakash, and G. V. Stenico, On the decaying-sterile neutrino solution to the electron (Anti)Neutrino appearance anomalies, arXiv:1911.01447.
[25] S. Hannestad, R. S. Hansen, and T. Tram, How Secret Interactions can Reconcile Sterile Neutrinos with Cosmology, Phys. Rev. Lett. **112**, 031802 (2014).
[26] B. Dasgupta and J. Kopp, A Ménage à Trois of eV-Scale Sterile Neutrinos, Cosmology, and Structure Formation, Phys. Rev. Lett. **112**, 031803 (2014).
[27] M. C. Gonzalez-Garcia, F. Halzen, and M. Maltoni, Physics reach of high-energy and high-statistics Icecube atmospheric neutrino data, Phys. Rev. D **71**, 093010 (2005).
[28] Z. Moss, M. H. Moulai, C. A. Argüelles, and J. M. Conrad, Exploring a nonminimal sterile neutrino model involving decay at IceCube, Phys. Rev. D **97**, 055017 (2018).
[29] M. C. Gonzalez-Garcia and M. Maltoni, Status of oscillation plus decay of atmospheric and long-baseline neutrinos, Phys. Lett. B **663**, 405 (2008).
[30] S. Gninenko, The MiniBooNE Anomaly and Heavy Neutrino Decay, Phys. Rev. Lett. **103**, 241802 (2009).
[31] S. N. Gninenko, A resolution of puzzles from the LSND, KARMEN, and MiniBooNE experiments, Phys. Rev. D **83**, 015015 (2011).
[32] E. Bertuzzo, S. Jana, P. A. N. Machado, and R. Zukanovich Funchal, A Dark Neutrino Portal to Explain MiniBooNE, Phys. Rev. Lett. **121**, 241801 (2018).
[33] P. Ballett, S. Pascoli, and M. Ross-Lonergan, U(1)' mediated decays of heavy sterile neutrinos in MiniBooNE, Phys. Rev. D **99**, 071701 (2019).
[34] J. R. Jordan, Y. Kahn, G. Krnjaic, M. Moschella, and J. Spitz, Severe Constraints on New Physics Explanations of the MiniBooNE Excess, Phys. Rev. Lett. **122**, 081801 (2019).
[35] O. Fischer, A. Hernandez-Cabezudo, and T. Schwetz, Explaining the MiniBooNE excess by a decaying sterile neutrino with mass in the 250 MeV range, Phys. Rev. D **101**, 075045 (2020).
[36] M. Lindner, T. Ohlsson, and W. Winter, A Combined treatment of neutrino decay and neutrino oscillations, Nucl. Phys. **B607**, 326 (2001).
[37] P. Huber, M. Lindner, and W. Winter, Simulation of long-baseline neutrino oscillation experiments with GLoBES, Comput. Phys. Commun. **167**, 195 (2005).
[38] J. Kopp, Efficient numerical diagonalization of Hermitian 3×3 matrices, Int. J. Mod. Phys. C **19**, 523 (2008); Erratum, Int. J. Mod. Phys. C **19**, 845 (2008).
[39] P. Huber, J. Kopp, M. Lindner, M. Rolinec, and W. Winter, New features in the simulation of neutrino oscillation experiments with GLoBES 3.0, Comput. Phys. Commun. **177**, 432 (2007).
[40] B. Armbruster *et al.* (KARMEN Collaboration), Upper limits for neutrino oscillations muon-anti-neutrino to electron-anti-neutrino from muon decay at rest, Phys. Rev. D **65**, 112001 (2002).
[41] N. Agafonova *et al.* (OPERA Collaboration), Search for $\nu_\mu \to \nu_e$ oscillations with the OPERA experiment in the CNGS beam, J. High Energy Phys. 07 (2013) 004.
[42] M. Antonello, B. Baibussinov, P. Benetti, E. Calligarich, N. Canci *et al.*, Experimental search for the LSND anomaly with the ICARUS LAr TPC detector in the CNGS beam, Eur. Phys. J. C **73**, 2345 (2013).
[43] C. Farese, Results from ICARUS, Proceeding of the Neutrino 2014 conference in Boston, slides available at https://indico.fnal.gov/materialDisplay.py?contribId=265&sessionId=18&materialId=slides&confId=8022 (2014).
[44] M. Antonello, B. Baibussinov, P. Benetti, F. Boffelli, A. Bubak *et al.*, Some conclusive considerations on the comparison of the ICARUS $\nu_\mu \to \nu_e$ oscillation search with the MiniBooNE low-energy event excess, arXiv:1502.04833.
[45] L. Borodovsky, C. Chi, Y. Ho, N. Kondakis, W.-Y. Lee *et al.*, Search for Muon-Neutrino Oscillations $\nu_\mu \to \nu_e$ ($\bar{\nu}_\mu \to \bar{\nu}_e$) in a Wide Band Neutrino Beam, Phys. Rev. Lett. **68**, 274 (1992).
[46] A. Diaz, C. A. Argüelles, G. H. Collin, J. M. Conrad, and M. H. Shaevitz, Where are we with light sterile neutrinos? arXiv:1906.00045.
[47] P. Adamson *et al.* (MINOS Collaboration), Search for Sterile Neutrinos in MINOS and MINOS+ Using a Two-Detector Fit, Phys. Rev. Lett. **122**, 091803 (2019).
[48] W. C. Louis, Problems With the MINOS/MINOS+ sterile neutrino muon-neutrino disappearance result, arXiv:1803.11488.
[49] D. A. Bryman and R. Shrock, Improved constraints on sterile neutrinos in the MeV to GeV mass range, Phys. Rev. D **100**, 053006 (2019).
[50] A. Atre, T. Han, S. Pascoli, and B. Zhang, The search for heavy majorana neutrinos, J. High Energy Phys. 05 (2009) 030.
[51] O. Dragoun and D. Vénos, Constraints on the active and sterile neutrino masses from beta-ray spectra: Past, present and future, J. Phys. **3**, 77 (2016).
[52] G. de André and A. Kobach, Global constraints on a heavy neutrino, Phys. Rev. D **93**, 033005 (2016).
[53] M. J. Dolinski, A. W. P. Poon, and W. Rodejohann, Neutrinoless double-beta decay: Status and prospects, Annu. Rev. Nucl. Part. Sci. **69**, 219 (2019).
[54] R. H. Cyburt, B. D. Fields, K. A. Olive, and T.-H. Yeh, Big bang nucleosynthesis: 2015, Rev. Mod. Phys. **88**, 015004 (2016).
[55] N. Aghanim *et al.* (Planck Collaboration), Planck 2018 results. VI. Cosmological parameters, arXiv:1807.06209.
[56] F.-Y. Cyr-Racine and K. Sigurdson, Limits on neutrino-neutrino scattering in the early universe, Phys. Rev. D **90**, 123533 (2014).
[57] F. Forastieri, M. Lattanzi, G. Mangano, A. Mirizzi, P. Natoli, and N. Saviano, Cosmic microwave background constraints on secret interactions among sterile neutrinos, J. Cosmol. Astropart. Phys. 07 (2017) 038.

[58] F. Forastieri, M. Lattanzi, and P. Natoli, Cosmological constraints on neutrino self-interactions with a light mediator, Phys. Rev. D **100**, 103526 (2019).

[59] M. Escudero and M. Fairbairn, Cosmological constraints on invisible neutrino decays revisited, Phys. Rev. D **100**, 103531 (2019).

[60] M. Escudero and S. J. Witte, A CMB search for the neutrino mass mechanism and its relation to the H_0 tension, Eur. Phys. J. C **80**, 294 (2020).

[61] L. Lancaster, F.-Y. Cyr-Racine, L. Knox, and Z. Pan, A tale of two modes: Neutrino free-streaming in the early universe, J. Cosmol. Astropart. Phys. 07 (2017) 033.

[62] I. M. Oldengott, T. Tram, C. Rampf, and Y. Y. Y. Wong, Interacting neutrinos in cosmology: Exact description and constraints, J. Cosmol. Astropart. Phys. 11 (2017) 027.

[63] N. Song, M. C. Gonzalez-Garcia, and J. Salvado, Cosmological constraints with self-interacting sterile neutrinos, J. Cosmol. Astropart. Phys. 10 (**2018**) 055.

[64] C. D. Kreisch, F.-Y. Cyr-Racine, and O. Doré, The neutrino puzzle: Anomalies, interactions, and cosmological tensions, Phys. Rev. D. **101**, 123505 (2020).

[65] N. Blinov, K. J. Kelly, G. Z. Krnjaic, and S. D. McDermott, Constraining the Self-Interacting Neutrino Interpretation of the Hubble Tension, Phys. Rev. Lett. **123**, 191102 (2019).

[66] I. Esteban, M. C. Gonzalez-Garcia, A. Hernandez-Cabezudo, M. Maltoni, and T. Schwetz, Global analysis of three-flavour neutrino oscillations: Synergies and tensions in the determination of θ_{23}, δ_{CP}, and the mass ordering, J. High Energy Phys. 01 (2019) 106; NuFIT 4.1, www.nu-fit.org (2019).

[67] E. Bertuzzo, S. Jana, P. A. N. Machado, and R. Zukanovich Funchal, Neutrino masses and mixings dynamically generated by a light dark sector, Phys. Lett. B **791**, 210 (2019).

[68] Y. Zhao, Cosmology and time dependent parameters induced by a misaligned light scalar, Phys. Rev. D **95**, 115002 (2017).

[69] X. Chu, B. Dasgupta, M. Dentler, J. Kopp, and N. Saviano, Sterile neutrinos with secret interactions—cosmological discord?, J. Cosmol. Astropart. Phys. 11 (2018) 049.

[70] Y. Farzan, Ultra-light scalar saving the $3+1$ neutrino scheme from the cosmological bounds, Phys. Lett. B **797**, 134911 (2019).

[71] E. W. Kolb and M. S. Turner, Supernova SN 1987a and the secret interactions of neutrinos, Phys. Rev. D **36**, 2895 (1987).

[72] J. M. Berryman, A. de Gouvea, and D. Hernandez, Solar neutrinos and the decaying neutrino hypothesis, Phys. Rev. D **92**, 073003 (2015).

[73] M. Maltoni and T. Schwetz, Testing the statistical compatibility of independent data sets, Phys. Rev. D **68**, 033020 (2003).

[74] J. Kostensalo, J. Suhonen, C. Giunti, and P. C. Srivastava, The gallium anomaly revisited, Phys. Lett. B **795**, 542 (2019).

[75] F. P. An *et al.* (Daya Bay Collaboration), Improved measurement of the reactor antineutrino flux and spectrum at Daya Bay, Chin. Phys. C **41**, 013002 (2017).

[76] T. Mueller, D. Lhuillier, M. Fallot, A. Letourneau, S. Cormon *et al.*, Improved predictions of reactor antineutrino spectra, Phys. Rev. C **83**, 054615 (2011).

[77] P. Huber, On the determination of anti-neutrino spectra from nuclear reactors, Phys. Rev. C **84**, 024617 (2011).

[78] V. Brdar, J. Kopp, and P. Machado, An Altarelli Cocktail for MiniBooNE: can a conspiracy of Standard Model effects explain the MiniBooNE anomaly? (to be published).